

A new and general method to calculate the drag force

Paulo Victor Santos Souza*

Instituto de Ciências Exatas, Universidade Federal Fluminense, Volta Redonda
Instituto Federal de Educação, Ciência e Tecnologia do Rio de Janeiro
Volta Redonda, Rio de Janeiro, Brazil

Daniel Girardi †

Departamento de Ciências Exatas e Licenciaturas, Campus Blumenau
Universidade Federal de Santa Catarina, Blumenau, Santa Catarina, Brazil

Paulo Murilo Castro de Oliveira‡

Instituto de Física, Universidade Federal Fluminense

Niterói, Rio de Janeiro, Brazil

Instituto Mercosul de Estudos Avançados, Universidade Federal da Integração Latino Americana
Foz do Iguaçu, Paraná, Brasil

1 de fevereiro de 2019

Abstract

We analyze the drag force acting on a cylinder in a wind tunnel. The inspiration comes from an experimental result: a small, light ball falls on air; its speed increases, reaches a maximum, decreases and finally stabilizes. This surprising breaking behavior is due to the gradual formation of the so-called von Kármán street of air vortices behind the ball: while it is not completely formed, the transient drag force is smaller than the known steady state value and the ball can reach speeds higher than its final value. To show it, we treat the similar problem of a cylinder inside a wind tunnel suddenly switched on, by solving the Navier-Stokes dynamic equation. We use a finite difference method with successive relaxations on a grid. We also treat the case of a rotating cylinder, leading to the Magnus force. The novelty is the method we

*paulo.victor@ifrrj.edu.br

†girardi1309@gmail.com

‡pmco@if.uff.br

use to calculate these forces, which avoids the traditional surface integration of velocity gradients; the latter demands a very precise determination of the velocity field near the cylinder or ball, a very hard numerical task.

Keywords: fluid dynamics, viscous flows, wind tunnels, drag force.

1 Introduction

The purpose of this paper is to introduce a totally new method (within the knowledge of the authors) to calculate the drag force on objects of any shape, immersed in fluid. This method, which can be implemented using any solution method for the Navier-Stokes equations, is here applied in the study of two different problems. The results, which are consistent with expectations, indicate that it is a reliable method, as the reader will see.

This work is motivated by a simple experiment, described in detail in (1): a polystyrene ball of diameter $\approx 2.5\text{cm}$ and mass $\approx 0.2\text{g}$ is released from some 3m above the floor, and the speed of fall is measured as function of time. Before stabilization, the speed reaches a maximum, and then decreases eventually reaching a steady state. The final, constant speed is $\approx 4\text{m/s}$, which corresponds to a Reynolds number $Re \approx 10^4$, thus already in the (periodic) turbulent regime, when the steady state drag force is known to be approximately proportional to the squared instantaneous speed. The force is then equal to the weight, being much larger than the negligible Stokes laminar drag force proportional to the speed itself. The authors propose that the conceptual explanation of the breaking fall lies in the gradual formation of successive turbulent air vortices behind the ball, which slowly go away, one after the other, the so-called von Kármán street, which is responsible for the above quoted turbulent drag force. The long street of vortices (a hundred diameters long) needs some transient time to be formed. During this transient, a sufficiently small and light ball under gravity alone can reach speeds larger than the (future) steady state value. Therefore, only after the street of vortices is completely formed, the falling ball gradually loses speed, until reaching its steady state constant value.

In this text, we apply the method described above to confirm this scenario, i.e., the existence of a transient drag force much smaller than its final steady state value. Besides the curious falling ball, this phenomenon is supposed to occur in many other dynamic systems where the Reynolds number rapidly increases with time, with potential applications. Here, we are interested only in explicitly exhibiting it, by adopting another dynamic system slightly similar to the falling ball. In order to do it, we calculate the drag force as a function of time: similarly to the speed, the force should be initially very small, later reaching a maximum value larger than its final steady state, before decreasing until it. Is this nearly frictionless initial transient followed by a maximum of the drag force confirmed by the calculations?

Instead of the ball, we adopt a long cylinder inside a wind tunnel, transversally positioned relatively to the wind. In this case, the originally three dimensional problem becomes two dimensional, simplifying the numerical effort. This simplification is justified by two arguments. First, the known steady state drag forces on a

cylinder or on a ball, as functions of the Reynolds number Re , present very similar behaviors, even quantitatively, when divided by the squared speed (the so-called drag coefficient). In particular, this coefficient remains approximately independent of the Reynolds number in the range from 10^3 until 10^5 , just the case of the experiment under study. This independence explains why the steady state drag force is proportional to the squared speed. Second, within the same range, the whole fluid velocity field $\mathbf{v}(\mathbf{r})$ around the cylinder remains almost perpendicular to it, and therefore can be considered a two dimensional field. The vorticity, $\boldsymbol{\Omega} = \nabla \times \mathbf{v}$ is always parallel to the cylinder, and can be considered a scalar field $\Omega(x, y, t)$. The starting configuration is windless, the wind tunnel switched off, i.e., Stokes laminar configuration obtained with $Re \rightarrow 0$ ¹. The wind is turned on at $t = 0$ with a fixed Reynolds number, say $Re = 1,000$, i.e., a suddenly fixed free-stream speed of the wind (or simply speed of the wind hereafter). Additionally, air density fluctuations do not appear in this case because all speeds are much smaller than the speed of sound ($\approx 330\text{m/s}$). Therefore we can set $\nabla \cdot \mathbf{v} = 0$.

This is not exactly the situation in the motivating experiment, where the Reynolds number (or the speed of the wind) gradually increases as the ball accelerates. Nevertheless, it presents just the same transient behavior, the street of vortices demanding some time to form. The numerical solution of the Navier-Stokes equation in dimensionless units (4)

$$\frac{\partial \Omega}{\partial t} = \frac{1}{Re} \nabla^2 \Omega - \nabla \times (\Omega \times \mathbf{v}) \quad (1)$$

follows the relaxation method (5) applied to the vorticity field².

The current text is organized as follows. Initially, we describe the method to determine the drag force. We apply it to the case of a fixed cylinder, where the drag force is parallel to the wind (possibly with very small angular fluctuations). Then, the same method is applied to the case of a rotating cylinder at constant angular speed, when the drag force becomes oblique, its transversal component is the so-called Magnus force. Finally, we present some conclusions.

2 General method to calculate the drag force

The traditional way to calculate the drag force from knowledge of the fluid velocity field around the cylinder (or any other rigid object) is based on the gradient of this field along the object/fluid surface. One must perform an integration over this surface. When the velocity field is determined at points of a discretized grid,

¹ To start with initial configuration already satisfying the Navier-Stokes equation (for $Re \rightarrow 0$) is crucial, otherwise, spurious transient behavior can be obtained (2). Also, Stokes problem in two dimensions presents a caveat: for strictly null Re and fixing the wind speed at infinite distances, no acceptable mathematical solution exists at large distances. For the realistic case of non null Re , this mathematical problem disappears. For a good discussion on that issue, see (3). Here, we simply fix a uniform and constant wind speed outside a 10×5 rectangle (in units of the cylinder diameter), covered by a 400×200 grid.

² A similar discussion can be seen in (6).

the accuracy in calculating the gradient is compromised, unless one adopts a very fine grid near the integration surface, which requires a lot of computer effort. In order to bypass this technical problem, we propose to replace the surface integral by a volume integral covering not only the object surface. Our argument is based on simple basic physics considerations, as follows.

We assume that there is a numerical method to determine the whole velocity field around the cylinder, on a discretized grid, as a function of time, i.e. a numerical method to solve the dynamic Navier-Stokes equation. It can be the relaxation method (5) adopted here, or any other method (references (7), (8), (9) or (10), for instance). The dynamic Navier-Stokes equation may be solved even by any adequate analytical approximation, if available in each case. At a time t the velocity field at each grid point \mathbf{r} is $\mathbf{v}_t(\mathbf{r})$. This configuration at time t is obtained from previous configurations at previous time steps $t-dt$, $t-2dt$, etc., obtained through the chosen method. At grid points inside the cylinder, $\mathbf{v}_t = 0$ at any time t .

Suppose the cylinder is removed at time t , and the volume the cylinder would occupy is filled with a static portion of fluid. Starting from the already known velocity field configuration $\mathbf{v}_t(\mathbf{r})$, the same method can be used in order to obtain a future configuration at time $t + Dt$. As the rigid cylinder is replaced by fluid, some non-null velocities appear inside the volume previously occupied by the cylinder. In other words, the removal of the cylinder allows the velocity field to penetrate a little bit inside its volume. Now, this internal velocity field can be integrated over the volume, the result multiplied by the fluid density, obtaining thus the total momentum which would be transferred from the fluid to the cylinder. Dividing this momentum by Dt one finally obtains the drag force at time t ³. There are other methods whose objective is to determine drag forces requiring the knowledge of the velocity field in a finite and arbitrarily chosen region enclosing the obstacle (11, 12). Our approach is completely different, instead of considering a volume outside the obstacle, we treat the internal volume occupied by the obstacle itself.

It is worth mention why the Newtonian momentum transfer procedure is enough in our case, no convective contributions are needed. There are two different descriptions to treat continuous fluid movements. The Lagrangian description takes the control volume of fluid moving with the fluid, the portion of fluid inside this volume is always the same, nothing entering or leaving this control volume. In this description, one can directly apply Newton's law. The Eulerian description takes a fixed and static control volume, the fluid passing through it. The relation between these two descriptions is made through the so-called convective derivatives. The material derivative (D/Dt) applicable to the Eulerian description is obtained by adding the quoted convective derivative ($v_x\partial/\partial x + v_y\partial/\partial y$) to the regular time derivative (d/dt) applicable to the Lagrangian description (13). This extra term is just the origin for convective corrections over merely Newtonian inertial forces. However, in our

³ The time Dt taken by the wind to enter the region previously occupied by the cylinder varies with the Reynolds number and with the initial conditions. We consider that an estimate of this time is acceptable, when multiplying it by 2, the transferred momentum becomes twice as large, with an error of no more than 6%. In the case of the static cylinder under $Re = 1,000$, we adopted Dt as the time the wind takes to transverse 0.1 grid pixel, the same dt adopted in the Navier-Stokes equation solution.

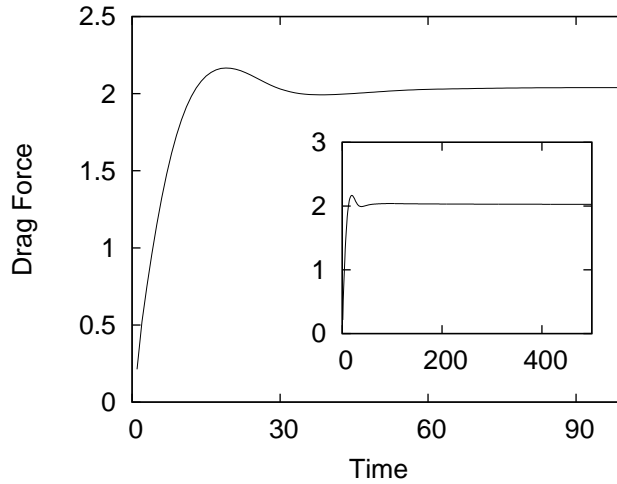


Figure 1 – Drag force on a static cylinder in the wind tunnel initially switched off. It is turned on at $t = 0$ with a constant Reynolds number $Re = 1,000$, which defines the speed of the wind. The force in the direction perpendicular to the wind flow is negligible. The dimensionless drag force is plotted in arbitrary units, ignoring factors as the fluid density, etc. During one time unit the wind travels one cylinder diameter. The force increases, reaches a maximum value, decreases and finally stabilizes, corresponding to a dynamic situation where successive vortices appear continuously, slowly going away, one running clockwise, the next running counterclockwise and so on. The long von Kármán street is then formed. Inset shows the same in a longer time scale.

particular case, by replacing the cylinder by static fluid, our control volume is that of the cylinder itself. Because the fluid is static at this precise time t , the Lagrangian and Eulerian volume controls are exactly the same, no translations between them ($\partial/\partial x = \partial/\partial y = 0$), therefore the convective derivative of any quantity vanishes. That is why convective terms don't enter in our momentum transfer formulation. This also applies to the case of a rotating cylinder.

Figure 1 shows the behavior of the drag force as a function of time. Analysis of the graph for $Re = 1,000$ shows that the drag force on the stationary cylinder increases, reaches a maximum value, decreases, and stabilizes. As expected, the same behavior of the falling ball (1) is found for this large Reynolds number, for which the long von Kármán street of successive vortices is present. On the other hand, for small values of Re , about a few dozens, for which instead of the long street periodically fed with new vortices only two vortices appear and stabilize behind the cylinder, the force does not present a maximum value before stabilization. Also, in this case the drag force is much smaller.

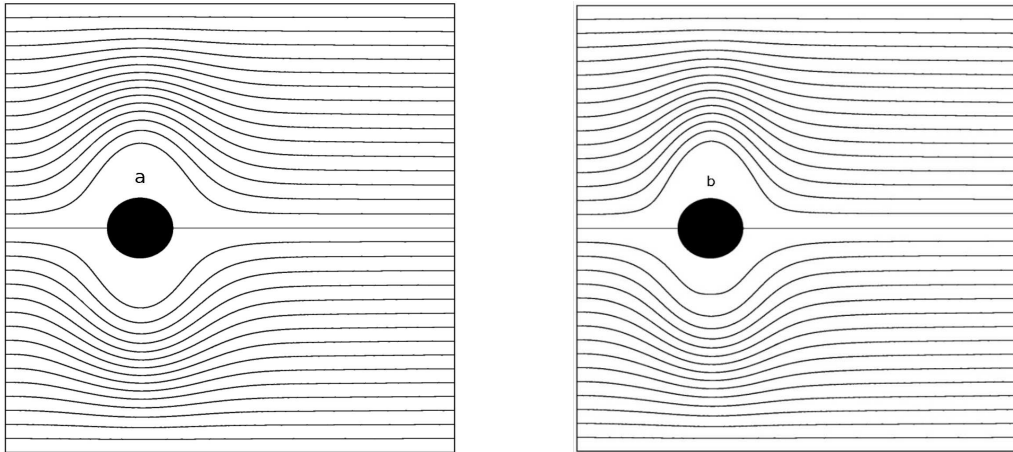


Figure 2 – Streamlines for Stokes’s configuration ($Re \rightarrow 0$), when the cylinder rotates clockwise with (a) $\omega = 0.1$ and (b) $\omega = 0.5$. The rotation of the cylinder results in the breakdown of the axial symmetry. As the angular speed increases, the lines are deformed, as expected. The wind goes from left to right.

3 Drag force on a rotating cylinder

In a different version of the problem, the cylinder rotates with constant angular speed ω . Now, the fluid velocities on the surface of the cylinder are not null, but are equal to the speed at the surface of the cylinder, i.e., the fluid rotates with the cylinder. The angular speed ω is measured in units such that $\omega = 1$ corresponds to the magnitude of the velocities on the surface of the cylinder equal to the speed of the wind.

Let’s start with the Stokes laminar limit ($Re \rightarrow 0$) for which the Navier-Stokes equation reduces to the Laplace equation, $\nabla^2 \Omega = 0$. The resulting streamlines are shown in figure 2.

When the original Navier-Stokes equation is solved for a fixed and large Reynolds number, say $Re = 1,000$, the solution shows that, after a transient time, the system cyclically stabilizes: a vortex rotating in the counterclockwise direction appears in the region behind the cylinder and below the horizontal axis formed by its diameter, see figure 3(a); then, this vortex grows and slowly moves away downstream; after some time, a second vortex appears in the region above the horizontal axis, rotating in the clockwise direction, see figure 3(b); this vortex also grows and moves away; later, a third vortex rotating in the counterclockwise direction begins to form in the region below the horizontal axis, see figure 3(c); and this process repeats again and again.

The method to determine the behavior of the drag force, presented in section 2, can be applied to the case of the rotating cylinder with one difference: the volume occupied by the cylinder is initially filled by fluid moving exactly as the cylinder, i.e., rotating as a rigid body at time t . Then, starting from this configuration, the flow evolves up to $t + Dt$.

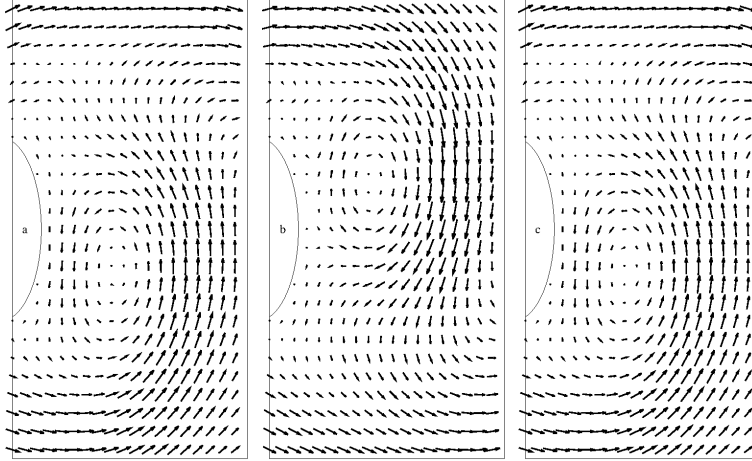


Figure 3 – Starting with Stokes’s laminar configuration for the clockwise rotating cylinder, the wind is switched on at $t = 0$, with a fixed Reynolds number $Re = 1,000$ and $\omega = 0.5$. After a transient time, the velocity field changes continually and periodically. Figure (a) shows a vortex that has just formed behind the cylinder, rotating in the counterclockwise direction. It then moves away to the right. Some time later, another vortex is formed behind the cylinder, rotating in the clockwise direction, figure (b). Later, figure (c), the velocity field returns to the configuration observed in figure (a). The whole process is periodically repeated. At this fine scale close to the cylinder back side, the behavior is the same observed in the case of a fixed cylinder. However, behind this region there is a long von Kármán street of already previously formed vortices, now bended downwards in this slowly rotating case considered here.

In this case, due to rotation, the force on the cylinder has a non zero component in the direction transverse to the wind, as shown in figure 4. The emergence of the transversal non-zero component is due to an asymmetry in the boundary layer⁴ separation, triggered first near the bottom of the cylinder (as in figures 2 and 3, the cylinder is considered to rotate clockwise). This is a clear manifestation of the well known Magnus effect⁵. As a net result, the von Kármán street as a whole is deflected downwards, explaining the non null average in figure 4, curve (b), and figure 5. The oscillations are due to the appearance of successive vortices spinning in alternate senses, forming the street. Close to the cylinder, a counterclockwise vortex pushes it downwards, subtracting an extra force from the average value, see figure 3(a) corresponding to a minimum of the Magnus force in figure 4(b). A clockwise vortex, see figure 3(b), pushes the cylinder upwards, adding an extra force to the average, corresponding to a maximum of figure 4(b). It is interesting to observe that

⁴ The boundary-layer results from the adherence of the air molecules to the object, say a cylinder. Due to viscosity, the adherence is partially transmitted to the molecules situated farther from the cylinder; this defines a region that moves with the cylinder, called boundary-layer or layer of Prandtl. See, for instance, (14).

⁵ More details can be found in (15).

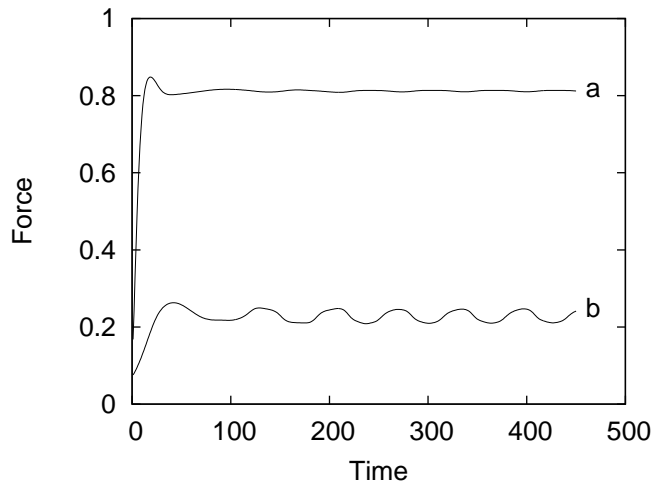


Figure 4 – The drag force on a rotating cylinder inside the wind tunnel with Reynolds number $Re = 1,000$, and $\omega = 0.1$. The parallel-to-the-wind component of the drag force (a) shows the same behavior as before, in the case of fixed cylinder. During the transient stage, the transverse-to-the-wind component of the force (b) also increases, reaches a maximum, and decreases. However, this component does not stabilize. Instead, it oscillates around a mean value. The oscillation is due to the alternate formation of counterclockwise and clockwise vortices, being a signature of the von Kármán street. For small values of Re , up to a few dozens, both components of the drag force don't oscillate, a signature of the absence of successive vortices.

the parallel-to-the-wind component also oscillates, hardly visible in figure 4, curve (a) (see also (2, 16)).

For larger angular speeds ($\omega \approx 2.5$), it is known that the street of vortices disappears (17, 18, 19, 20, 21, 22). Figure 6 (top) shows the behavior of the transverse-to-the-wind component of the force for some values of ω larger than before. As expected, the oscillations are attenuated over time and tend to disappear for $\omega \approx 2.5$, but reappear for $\omega \approx 4.5$. Indeed, according to reference (19), for Reynolds numbers a little bit smaller, the flow becomes unstable again inside a window around $\omega \approx 4.5$.

In figure 6 (bottom), it is shown the behavior of the parallel-to-the-wind component of the force. This component is very small due to the absence of a vortex street, except, again as before, inside the quoted window (19), when the oscillations and the street reappear.

4 Final Remarks

In this paper, we introduce a method to determine the dynamic behavior of the drag force acting on an object inside a wind tunnel. Initially, the wind is turned

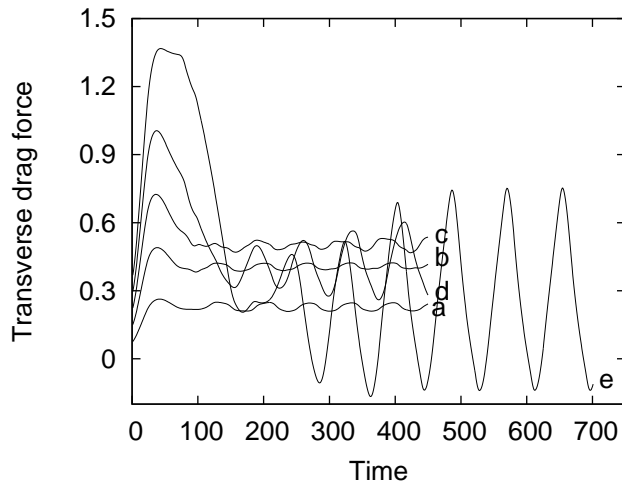


Figure 5 – Transverse-to-the-wind component of the force as a function of time, for various small angular speeds of the rotating cylinder with $Re = 1,000$: (a) $\omega = 0.1$; (b) $\omega = 0.2$; (c) $\omega = 0.3$; (d) $\omega = 0.4$; and (e) $\omega = 0.5$. After the transient stage, the Magnus force oscillates around an average value.

off, and suddenly turned on with a fixed Reynolds number, i.e., with a constant wind speed, which is maintained thereafter. In the case of a static cylinder, the force increases, reaches a maximum value, decreases and stabilizes. This behavior agrees with the experimental results presented in (1).

In the case of a slowly rotating cylinder, the component of the drag force parallel to the wind flow behaves in the same way as in the case of the cylinder at rest. However, the transverse-to-the-wind component is not null: it grows, reaches a maximum, decreases and fluctuates around a non null value. This is a clear manifestation of the well known Magnus effect. Moreover, also in this case, the method is even capable of identifying a transition scheme where the von Kármán street of vortices disappears, reappears and disappears again for increasing rotational speeds.

5 Acknowledgments

This work is partially supported by the Brazilian agencies CAPES and CNPq. The authors thank P.M.C. Dias for her comments on this work.

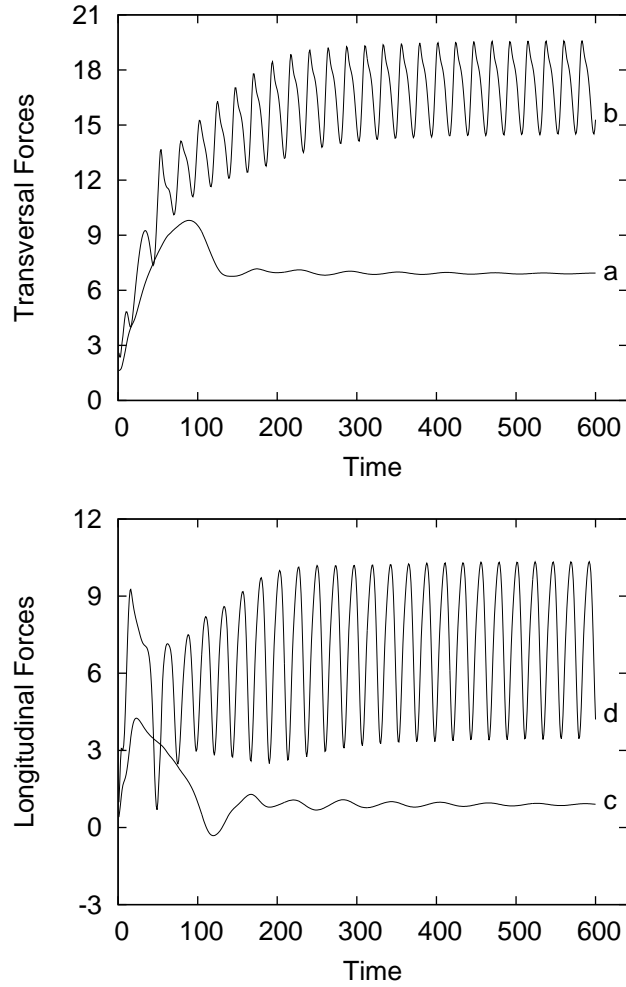


Figura 6 – On the top, we show the transverse-to-the-wind component of the drag force for $\omega = 2.5$ (a) and $\omega = 4.5$ (b). When $\omega \approx 2.5$, the oscillations are attenuated over time and tend to disappear, due to the absence of the von Kármán street. However, in (b), when $\omega \approx 4.5$, the oscillations (and the street) are present again. On the bottom, we show the parallel-to-the-wind component of the drag force for $\omega = 2.5$ (c) and $\omega = 4.5$ (d). Note that this component is very small for $\omega \approx 2.5$. But, in (d), when $\omega \approx 4.5$, as before, the flow is unstable again and the oscillations reappear around a larger average value.

Referências

- 1 OLIVEIRA, P. M. C. de et al. Can a falling ball lose speed? *arXiv preprint arXiv:1005.4086*, 2010.
- 2 CRUCHAGA, M. A. et al. Computing past cylinder flows. *Mecánica Computacional*, XXI, p. 462–475, 2002.
- 3 CHILDRESS, S. *An introduction to theoretical fluid mechanics*. [S.l.]: Courant Institute of Mathematical Sciences, 2009.
- 4 FEYNMAN, R. P.; LEIGHTON, R. B.; SANDS, M. *The Feynman lectures on physics. 2 (1969). Mainly electromagnetism and matter*. [S.l.]: Addison-Wesley, 1969.
- 5 OLIVEIRA, P. M. C. de. Relaxation method for Navier-Stokes equation. *International Journal of Modern Physics C*, World Scientific, v. 23, n. 04, 2012.
- 6 INOUE, O.; YAMAZAKI, T. Secondary vortex streets in two-dimensional cylinder wakes. *Fluid Dynamics Research*, Elsevier, v. 25, n. 1, p. 1–18, 1999.
- 7 ENGELMAN, M. S.; JAMNIA, M. Transient flow past a circular cylinder: a benchmark solution. *International Journal for Numerical Methods in Fluids*, Wiley Online Library, v. 11, n. 7, p. 985–1000, 1990.
- 8 ALFONSI, G.; GIORGINI, A. Temporal evolution of high-order vortices in the nonsymmetric wake past a circular cylinder. *Fluid Dynamics Research*, Elsevier, v. 31, n. 1, p. 13–39, 2002.
- 9 SUH, J.-C.; KIM, K.-S. A vorticity–velocity formulation for solving the two-dimensional navier–stokes equations. *Fluid Dynamics Research*, Elsevier, v. 25, n. 4, p. 195–216, 1999.
- 10 PESAVENTO, U.; WANG, Z. J. Falling paper: Navier-Stokes solutions, model of fluid forces, and center of mass elevation. *Physical Review Letters*, APS, v. 93, n. 14, p. 144501, 2004.
- 11 NOCA, F.; SHIELS, D.; JEON, D. A comparison of methods for evaluating time-dependent fluid dynamic forces on bodies, using only velocity fields and their derivatives. *Journal of Fluids and Structures*, Elsevier, v. 13, n. 5, p. 551–578, 1999.
- 12 TAN, B. T.; THOMPSON, M. C.; HOURIGAN, K. Evaluating fluid forces on bluff bodies using partial velocity data. *Journal of Fluids and Structures*, Elsevier, v. 20, n. 1, p. 5–24, 2005.
- 13 SCHNEIDERBAUER, S.; KRIEGER, M. What do the Navier-Stokes equations mean? *European Journal of Physics*, IOP Publishing, v. 35, n. 1, p. 015020, 2014.

- 14 AGUIAR, C.; RUBINI, G. A aerodinâmica da bola de futebol. *Revista Brasileira de Ensino de Física*, v. 26, p. 297–306, 2004.
- 15 ALAWAYS, L. W. *Aerodynamics of the curve-ball: an investigation of the effects of angular velocity on baseball trajectories*. Tese (Doutorado) — University of California Davis, 1998.
- 16 Lu, X.-Y. Numerical study of the flow behind a rotary oscillating circular cylinder. *International Journal of Computational Fluid Dynamics*, v. 16, p. 65–82, 2002.
- 17 Chen, Y.-M.; Ou, Y.-R.; Pearlstein, A. J. Development of the wake behind a circular cylinder impulsively started into rotatory and rectilinear motion. *Journal of Fluid Mechanics*, v. 253, p. 449–484, ago. 1993.
- 18 STOJKOVIĆ, D.; BREUER, M.; DURST, F. Effect of high rotation rates on the laminar flow around a circular cylinder. *Physics of Fluids*, v. 14, p. 3160–3178, 2002.
- 19 MITTAL, S.; KUMAR, B. Flow past a rotating cylinder. *Journal of Fluid Mechanics*, v. 476, p. 303 – 334, 2003.
- 20 KALININ, E. I.; MAZO, A. B. Steady and periodic regimes of laminar flow around the rotating cylinder. *TsAGI Science Journal*, Begel House Inc., v. 42, n. 5, 2011.
- 21 RAO, A. et al. Three-dimensionality in the wake of a rotating cylinder in a uniform flow. *Journal of Fluid Mechanics*, v. 717, p. 1–29, 2 2013. ISSN 1469-7645.
- 22 RAO, A. et al. A review of rotating cylinder wake transitions. *Journal of Fluids and Structures*, v. 53, p. 2–14, 2014.